communications earth & environment

Article

https://doi.org/10.1038/s43247-024-01819-4

Fast-get-faster explains wavier upper-level jet stream under climate change

Tiffany A. Shaw [1] ✉, Osamu Miyawaki [2], Hsing-Hung Chou [1] & Russell Blackport [3]

Earth's upper-level jet streams primarily flow in the eastward direction. They often exhibit a north-south component or waviness connected to extreme weather at the surface. Recently the upper-level eastward jet stream was found to exhibit a fast-get-faster response under climate change explained by the impact of the nonlinear Clausius-Clapeyron relation on the latitudinal density contrast. Here we show the fast-get-faster mechanism also applies to the upper-level north-south jet stream wind and the longitudinal density contrast, implying increased waviness under climate change. Arctic Sea ice loss, which has been proposed as a driver of increased waviness, cannot explain the response. It leads to a fast-get-slower waviness response at all vertical levels. We demonstrate the fast-get-faster waviness signal has emerged in reanalysis data in the Southern Hemisphere but not yet in the Northern Hemisphere. The results show the fast-get-faster mechanism explains upper-level waviness changes and highlights a tug of war between upper- and mid-level waviness under climate change.

Earth's upper-level jet streams are narrow bands of wind that primarily flow in the eastward direction consistent with their existence being tied to differential heating between the equator and pole along with Earth's rotation[1–3]. The eastward jet frequently exhibits a north-south (meridional) component associated with Rossby waves and high and low pressure weather systems, hereafter referred to as jet stream waviness. The connection between jet stream waviness and meridional wind is consistent with both vanishing in the axially symmetric (longitudinally independent) limit where the jet stream is purely in the eastward direction with no meridional component and thus no waviness[4]. Furthermore, many metrics used to quantify waviness have zero or minimum waviness corresponding to purely eastward flow[5–8]. Jet stream waviness is important because it has been connected to regional surface temperature extremes and air quality[9–15]. This is consistent with the jet stream representing the boundary between air of contrasting densities (warm, moist and light air near the equator and cold, dry and dense air near the pole).

Recently, the eastward component of the upper-level jet stream was shown to exhibit a fast-get-faster response under climate change[16]. In particular, fast (>99th percentile) upper-level eastward jet stream winds increased 2.5 times more than the average eastward jet stream wind under climate change. This behavior followed from a multiplicative increase of ~2% per degree of global mean change in surface air temperature. It was explained from the impact of the nonlinear Clausius-Clapeyron (CC) relation on the latitudinal density contrast via moist thermal wind. The intuition behind the mechanism comes from the tropics "holding" more moisture than the poles because they are warmer due to differential heating between the equator and pole. Under climate change the density contrast gets steeper because warmer air "holds" more moisture following the CC relation [see Fig. 3 in[16,17]]. Importantly, the fast-get-faster mechanism depended on the CC relation and historical latitudinal temperature contrasts, the change in latitudinal temperature contrast under climate change (e.g. Arctic amplification) was a second order effect. The results indicate that climate change strongly affects the tails of the upper-level (250 hPa) daily jet stream wind distribution. This has important implications for commercial flight times, record-breaking winds, clear-air turbulence and severe weather occurrence under climate change.

The mechanism underlying the fast-get-faster response of upper-level eastward jet stream wind should also affect the meridional jet stream wind. The meridional jet stream wind is connected to longitudinal density contrasts driven by Rossby waves and low and high pressure weather systems. For example, a fast southward upper-level jet stream wind over the continental US (discussed further below) is associated with a large longitudinal near-surface temperature contrast (warm air to the west of the star and cold air to east, Fig. 1a). Following the intuition mentioned above, the air to the west of the fast southward wind "holds" more moisture than the air to the east because it is warmer (288 K versus 257 K, blue line, Fig. 1c). Under climate change the density contrast gets steeper following the multiplicative CC relation (solid blue to orange lines, Fig. 1c). The same intuition holds for the mean southward wind but since the mean density contrast is smaller to begin with (Fig. 1b) its increase is less (dashed blue to

[1]Department of the Geophysical Sciences, The University of Chicago, Chicago, IL, USA. [2]Climate and Global Dynamics Laboratory, National Center for Atmospheric Research, Boulder, CO, USA. [3]Canadian Centre for Climate Modelling and Analysis, Environment and Climate Change Canada, Victoria, BC, Canada. ✉e-mail: tas1@uchicago.edu

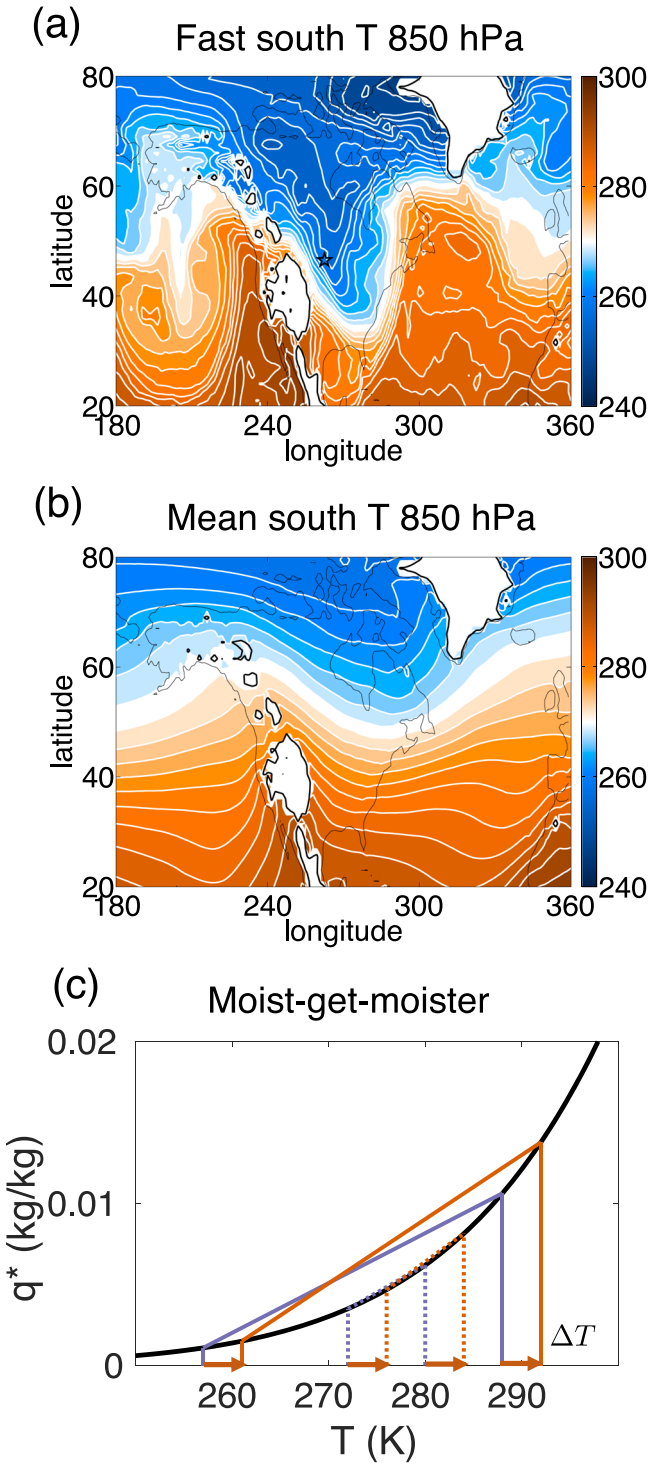

Fig. 1 | Response of longitudinal density contrasts under climate change following the Clausius-Clapeyron relation. Near-surface (850 hPa) temperature corresponding to upper-level (250 hPa) (**a**) fast (star, see Fig. 2c, d) and (**b**) mean southward jet stream wind over the continental US. **c** Near-surface air to the west of the star in (**a**) "holds" more moisture than the air to the east following the Clausius-Clapeyron relation (black line) in the historical climate (slope of blue line from representative temperatures on the west 288 K and east 257 K side of the star at 46.5°N from (**a**)). Under climate change (warming of 4K) the longitudinal contrast of saturation-specific humidity increases implying a steeper density contrast (solid orange line is steeper than solid blue line). A similar result holds for the mean temperature contrast (**b**) but the contrast does not increase as much because it is smaller to begin with (dashed orange line is slightly steeper than dashed blue line).

orange lines, Fig. 1c) consistent with the nonlinear CC relation. This shows the moist-get-moister CC mechanism amplifies all density contrasts regardless of their origin and hence dynamically driven longitudinal density contrasts should get steeper under climate change, implying increased upper-level jet stream waviness all else being equal. Thus, the fast-get-faster mechanism might provide an explanation for jet stream waviness changes under climate change.

How waviness is changing now and how it will change in the future is actively debated in the literature[18–21]. Here we highlight a few important results in the context of waviness changes and the fast-get-faster mechanism. It is currently unclear how waviness changes at upper levels (e.g. 250 hPa) under climate change where the fast-get-faster mechanism applies because previous work has mostly focused on mid-level waviness (500 hPa or ~5 km above the surface). Previous work demonstrated a robust weakening of mid-level waviness under climate change[6,22,23]. Significant linear trends in mid-level waviness in the satellite era have been difficult to detect, especially during Northern Hemisphere wintertime[24,25]. However, a decrease in temperature variability has clearly emerged in observed trends[16,26] noted that the density contrast at lower levels is dominated by different factors than at upper levels, including moist adiabatic adjustment (see their Fig. S2), and thus the moist thermal wind relation may also help to explain the decrease in mid-level waviness.

The physical mechanisms that have been proposed to explain waviness changes under climate change include the following. Arctic Sea ice loss and Arctic amplification of surface warming, which are robust and well-understood consequence of climate change[27–29], have been proposed to increase waviness following a slow down the eastward jet stream[5,30]. Land-ocean heating asymmetries have also been suggested to increase waviness[31]. On the other hand it has been suggested that temperature variability will decrease in response to Arctic warming following temperature advection arguments[13,32]. Uncovering the mechanisms underlying the climate change response is important for having confidence in climate model projections[19,33–36].

Here we investigate how the fast-get-faster mechanism affects the meridional jet stream wind under climate change and thereby waviness at different vertical levels across a hierarchy of climate models from the World Climate Research Programme's Coupled Model Intercomparison Project Phase 6 (CMIP6)[37]. The fast-get-faster mechanism operates daily, at each horizontal grid point (longitude and latitude) thus we focus on local jet stream waviness changes under climate change. We consider the impact of the fast-get-faster mechanism on waviness metrics that can be defined locally, including meridional wind, Meridional Circulation Index (MCI)[5] and Local Wave Activity (LWA)[38]. Metrics based on the length of a contour[6,8] cannot be defined locally (they do not depend on longitude) and thus cannot be easily connected to the fast-get-faster response.

The connection between the tails of the meridional wind distribution, waviness and jet stream wind is illustrated using historical (1980 to 2000) examples. Over the Pacific, a fast northward wind (v >99.9th percentile) reaches ~80 ms^{-1} (star, Fig. 2a, b) and couples to southward wind downstream consistent with an omega block in the jet stream wind ($\sqrt{u^2+v^2}$, Fig. 2b). Along similar lines, over the continental US a fast southward wind (v < 0.1th percentile) reaches ~ −70 ms^{-1} and couples to northward flow up and downstream (star, Fig. 2c, d) consistent with a Rossby wave packet in the jet stream wind (Fig. 2d). Thus, the tails of the meridional wind distribution are associated with local synoptic features, e.g. Rossby wave packets[39] and blocking anticyclones[40] and not with circumglobal waviness.

Local regions of weak jet stream wind speed (e.g., around 65°N, 150°E in Fig 2b and 50°N, 210°E in Fig. 2d) are problematic features for MCI (Supplementary Fig. 1a, b). They interfere with the interpretation that high values of MCI correspond to a wavier jet stream. Similarly, LWA does not maximize where the jet stream wind maximizes (Supplementary Fig. 1c, d) because it depends on the geopotential height, which is related to the jet stream wind through a spatial gradient. Thus, neither MCI or LWA are good

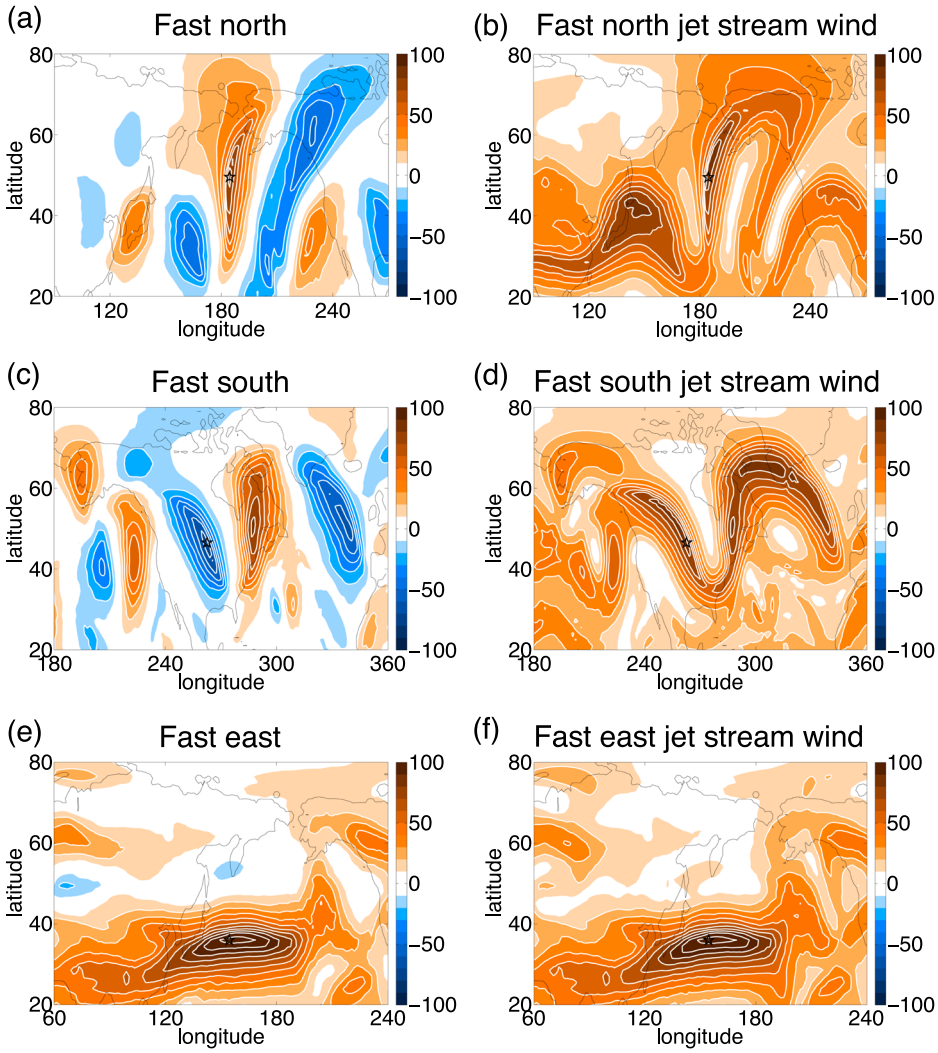

Fig. 2 | Fast upper-level jet stream wind. Example of fast upper-level (250 hPa) (**a**) northward, (**c**) southward and (**e**) eastward wind (ms^{-1}) at location indicated by the black star. **b**, **d**, **f** The corresponding jet stream wind ($\sqrt{u^2+v^2}$, ms^{-1}).

metrics of fast meridional jet stream winds and they cannot be easily related to the fast-get-faster mechanism.

In contrast to fast meridional wind, a fast eastward wind (u > 99.9th percentile) involves a jet streak with eastward wind exceeding 110 ms^{-1} (star, Fig. 2e, f) with no obvious jet stream waviness (Fig. 2f). Once again MCI or LWA are not good metrics of fast eastward jet stream winds (Supplementary Fig. 2). Ultimately, fast upper-level jet stream winds involve distinct features, which is consistent with the eastward and meridional components of the jet stream wind being uncorrelated on the daily timescale at individual spatial locations (Supplementary Fig. 3).

In what follows we focus on extratropical (45 to 90° latitude) waviness in the upper (250 hPa) and mid (500 hPa) troposphere following previous work[6,16,24,25]. In order to quantify the response to anthropogenic forcing, we quantify the daily, local (defined at each latitude and longitude) waviness distribution at the end of the 20th (1980 to 2000) and 21st (2080 to 2100) centuries under a high emission scenario (SSP5-8.5). When examining near-term trends we also consider a lower emission scenario (SSP2-4.5). The historical distribution of extratropical upper-level waviness defined using daily meridional wind is close to symmetric about zero exhibiting fast northward and southward tails in reanalysis data[41] (red line, Supplementary Fig. 4a). The distribution is similar between the extended winter and summer seasons (Supplementary Fig. 5). Climate models capture the waviness distribution in reanalysis data reasonably well (black and red lines, Supplementary Fig. 4a). The mid-level waviness distribution exhibits a similar structure to upper-level waviness but its amplitude is smaller (Supplementary Fig. 4b).

Results

Fast upper-level meridional winds get faster

Climate models project fast upper-level meridional jet stream winds get faster. In particular, the fast tails increase ~3 times more than the response of the average of the absolute value of upper-level meridional wind under climate change (black line, Fig. 3a). This increase of fast upper-level meridional jet stream wind implies increased waviness. The fast-get-faster response of the meridional wind is consistent with all days in the extratropical (45–90°) waviness distribution increasing at a rate of ~2% per degree of global-mean change in surface air temperature, hereafter ~2%/K (Supplementary Fig. 6). (Subtropical and tropical waviness decrease at a rate of ~1%/K under climate change.) More specifically, if each day in the end of the 20th century meridional jet stream wind distribution is multiplied by ~2%/K times the global-mean warming of surface air temperature the wavy-get-wavier response emerges (red line, Fig. 3a). (Note each model response is calculated separately using its own global-mean change in surface air temperature.) Thus, the fast upper-level meridional jet stream wind distribution involves a multiplicative (percent) increase under climate change and not an additive increase (shift of the entire distribution) toward increased waviness. Hereafter we refer to this as the fast-get-faster response of upper-level jet stream waviness.

The fast-get-faster response of upper-level jet stream waviness is very robust and occurs in all models. Fast northward (>95th percentile) and southward (<5th percentile) winds increase ~3 times more than the average of the absolute value in both hemispheres (see NH and SH in Fig. 3b), across the seasonal cycle (see winter Win, selected months, and summer Sum,

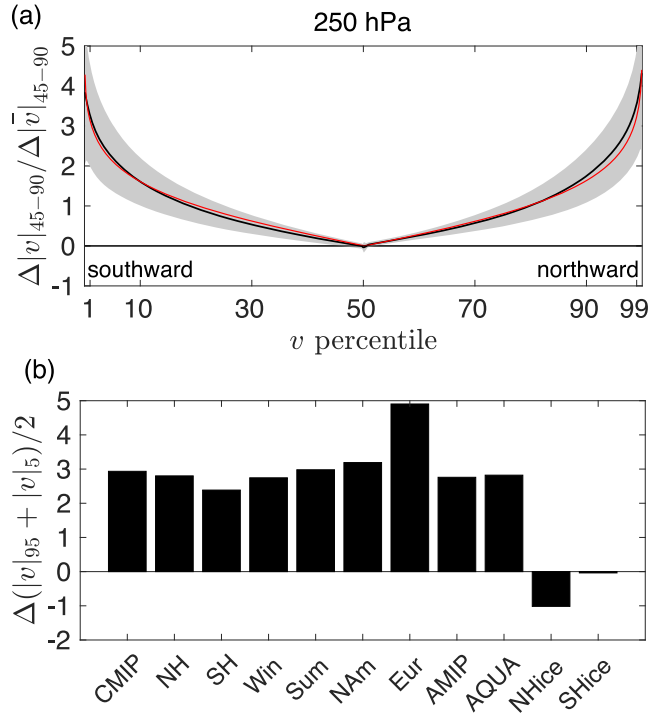

Fig. 3 | Wavy upper-level jet stream winds under climate change. a Response of the extratropical (45–90°) upper-level (250 hPa) jet stream waviness distribution in both hemispheres across percentiles relative to the average of the absolute value of upper-level waviness ($|\overline{v}|$). The red line indicates the prediction following an increase of 2% per degree of surface air temperature change times the late 20th century distribution. Data are presented as multi-coupled-model-mean (black line) ± one standard deviation of the response across the model ensemble (shading). **b** Multi-model mean amplification of extreme waviness (average of response for >95th and <5th percentiles) relative to the average of the absolute value of upper-level waviness ($|\overline{v}|$) for coupled models for different hemispheres (NH and SH), different seasons (Win, selected months, and Sum, selected months), across different longitudinal sectors (North America NAm 180°W–140°W and Eurasia Eur 40°W–180°E), across different model configurations (coupled CMIP, uncoupled AMIP, aquaplanet AQUA) and in response to Arctic Sea ice loss in the Northern and Southern Hemispheres (NHice and SHice).

selected months in Fig. 3b), across different longitudinal sectors in the Northern Hemisphere (see North America NAm 180°W–140°W and Eurasia Eur 40°W–180°E in Fig. 3b) and in response to uniform sea surface temperature warming in simpler models without coupling to the ocean or land (see AMIP and AQUA in Fig. 3b). The robustness of the fast-get-faster response of upper-level jet stream waviness suggests it is tied to a robust underlying physical mechanism.

The results above establish that the fast-get-faster response occurs for both eastward and meridional components of the upper-level jet stream wind. The fast-get-faster eastward wind response represents increased jet streaks whereas the fast-get-faster meridional wind response represents increased waviness. MCI cannot capture the response of extremes because the index is bounded by ±1 (Supplementary Fig. 7a). Interestingly, the eastward and meridional wind fast-get-faster signals lead to competing influences on upper-level MCI under climate change. In particular, the numerator increases consistent with the fast-get-faster meridional wind response (Supplementary Fig. 7b). In contrast, MCI decreases because the denominator increases consistent with the fast-get-faster eastward wind response (Supplementary Fig. 7c) dominating the jet stream wind ($\sqrt{u^2+v^2}$). Extreme upper-level LWA increases under climate change (black line, Supplementary Fig. 8a) but the response is not robust across the model ensemble (shading, Supplementary Fig. 8a).

The fast-get-faster upper-level meridional wind response represents increased waviness under climate change. Previous studies suggested Arctic sea ice loss, Arctic amplification[5,30] and Northern Hemisphere land-sea thermal forcing contrast[31] drive increased waviness under climate change. However, the fast-get-faster response of upper-level waviness emerges in response to uniform sea surface temperature warming in longitudinally-symmetric aquaplanet simulations without Arctic Amplification and land-sea contrast (Supplementary Fig. 9) suggesting those factors are not essential. In order to quantify the impact of Arctic Sea ice loss we use targeted climate model simulations that impose end-of-century Arctic sea ice loss without changes in greenhouse gases[42,43] (see Methods). In response to Arctic Sea ice loss fast upper-level meridional winds get slower in the Northern Hemisphere with no significant change in the Southern Hemisphere (see NHice, SHice in Figs. 3b). This shows Arctic Sea ice loss also does not drive the fast-get-faster response of upper-level waviness. Arctic sea ice loss is associated with a fast-get-slower waviness response. A similar result is found for the extratropical eastward jet stream wind in response to Arctic sea ice loss.

As mentioned above, the CC mechanism underlying the fast-get-faster upper-level eastward jet stream wind response should also affect the meridional jet stream wind. Here we quantify the connection between the fast-get-faster upper-level meridional wind response and the CC mechanism. The meridional wind can be connected to longitudinal density contrasts from the surface to the upper-level and thus to CC via moist thermal wind, e.g.

$$\begin{aligned} v_{Tm} &\equiv -\int_{p_s}^{250\,\mathrm{hPa}} \frac{1}{fa\cos\phi}\frac{\partial\alpha(s^*,p)}{\partial\lambda}dp \\ &= -\int_{p_s}^{250\,\mathrm{hPa}} \frac{1}{fa\cos\phi}\left(\frac{\partial T}{\partial p}\right)_{s^*}\frac{\partial s^*}{\partial\lambda}dp \end{aligned} \quad (1)$$

where p_s is surface pressure, f is the Coriolis parameter, a is the radius of Earth, $\alpha = 1/\rho$ is the specific volume where ρ is density, ϕ is latitude, λ is longitude, p is pressure, $(\partial T/\partial p)_{s^*}$ is the moist adiabatic lapse rate in pressure coordinates, $s^* = c_p \ln\theta_e^*$ is the saturation (moist) entropy and θ_e^* is the equivalent potential temperature air would have if it were saturated at the same temperature and pressure. Saturation entropy is the sum of dry entropy ($s_d = c_p \ln\theta$ where θ is potential temperature) and saturation specific humidity (q^*), i.e. $s^* = s_d + L_v q^*/T$ where L_v is the latent heat of vaporization. We neglect the surface wind in equation (1), which is small consistent with previous work[16,44].

Moist thermal wind can be derived by writing the specific volume α as a function of s^* and p and using a thermodynamic Maxwell relation [Methods,[45,46]]. We use daily temperature data to compute moist thermal wind v_{Tm} at each horizontal grid location (latitude and longitude) and aggregate it across all days and all longitudes at a given latitude. The connection between upper-level meridional wind and the longitudinal density contrast in equation (1) is consistent with the wind distribution being dominated by its geostrophic component (Supplementary Fig. 10a).

The upper-level meridional wind response under climate change can then be connected to the moist-get-moister, dry entropy gradient and moist adiabatic adjustment responses under climate change:

$$\begin{aligned} \Delta v_{Tm} &\approx -\frac{1}{fa\cos\phi}\int_{p_s}^{250\,\mathrm{hPa}}\left[\left(\frac{\partial T}{\partial p}\right)_{s^*}\Delta\left(\frac{\partial s^*}{\partial\lambda}\right)+\frac{\partial s^*}{\partial\lambda}\Delta\left(\frac{\partial T}{\partial p}\right)_{s^*}\right]dp \\ &\approx -\frac{1}{fa\cos\phi}\int_{p_s}^{250\,\mathrm{hPa}}\Bigg[\underbrace{\left(\frac{\partial T}{\partial p}\right)_{s^*}\Delta\left(\frac{\partial}{\partial\lambda}\left(\frac{L_v q^*}{T}\right)\right)}_{\textit{moist get moister}} \\ &\quad+\underbrace{\left(\frac{\partial T}{\partial p}\right)_{s^*}\Delta\left(\frac{\partial s_d}{\partial\lambda}\right)}_{\textit{dry entropy grad.}}+\underbrace{\frac{\partial s^*}{\partial\lambda}\Delta\left(\frac{\partial T}{\partial p}\right)_{s^*}}_{\textit{moist adiab. adj.}}\Bigg]dp \end{aligned} \quad (2)$$

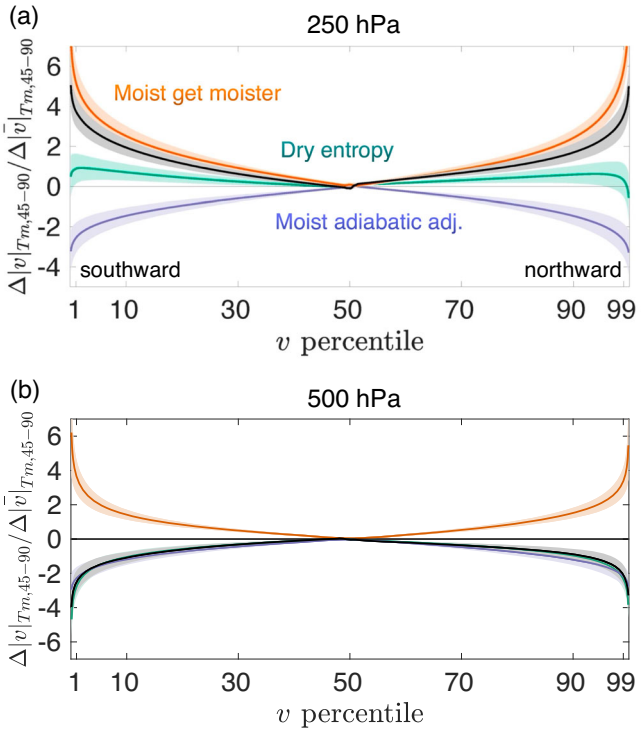

Fig. 4 | Relationship between fast-get-faster meridional wind response and moisture under climate change. Response of (**a**) upper-level (250 hPa) and (**b**) mid-level (500 hPa) moist thermal wind (black) over the extratropics (45–90° latitude) in both hemispheres across percentiles relative to the response of the average upper-level wind ($|\bar{v}_{Tm}|$) due to the contributions from moist-get-moister (orange), dry entropy gradient (green) and moist adiabatic adjustment (blue) responses (see equation (2)). Data are presented as multi-model-mean (thick line) ± one standard deviation of the response across the model ensemble (shading).

where Δ is the difference between the end of the 21st and 20th centuries. The residual in equation (2) is small confirming the usefulness of the moist thermal wind decomposition (Supplementary Fig. 11a).

The meridional component of upper-level moist thermal wind exhibits a fast-get-faster response under climate change (black line, Fig. 4a). The decomposition suggests the moist-get-moister contribution (first term on right hand side of (2)) is able to explain why fast meridional winds get faster under climate change (orange line, Fig. 4a). Thus, the fast-get-faster meridional wind response is connected to longitudinal density contrasts getting steeper under climate change (blue to orange lines Fig. 1c) similar to what was found for the eastward jet stream wind response and latitudinal density contrasts. In this case the longitudinal density contrasts, driven dynamically by Rossby waves and high and low pressure systems, get steeper. These contrasts occur historically and in the future but in the future they are amplified by the CC mechanism.

The amplified longitudinal density contrasts in the future could also be affected by changes in the horizontal temperature (and moisture) contrasts through a feedback between thermodynamics and dynamics. For example, faster meridional winds could lead to enhanced meridional transport of temperature and moisture further steepening the density contrast and amplifying the meridional wind. This interaction seems to be a second order effect because the fast-get-faster meridional wind emerges in response to vertically-varying global-mean warming with no change in horizontal temperature gradient (Supplementary Fig. 11b). It is also consistent with the fast-get-faster response of upper-level waviness emerging given the historical meridional wind distribution and a multiplicative increase of 2%/K (given only the change in global-mean surface air temperature with no change in temperature gradient, red line Fig. 3a). The small impact of the horizontal temperature gradient response on the moist-get-moister response is also consistent with the dominance of saturation specific humidity changes over temperature changes, i.e.

$$\Delta\left(\frac{\partial}{\partial\lambda}\left(\frac{L_v q^*}{T}\right)\right) = \frac{L_v q^*}{T}\left[\frac{1}{q^*}\frac{\partial\Delta q^*}{\partial\lambda} - \frac{1}{T}\frac{\partial\Delta T}{\partial\lambda}\right] \approx \frac{L_v}{T}\frac{\partial\Delta q^*}{\partial\lambda} \quad (3)$$

since $\Delta q^*/q^* \approx 28\% > \Delta T/T \approx 1\%$ for a 4 K global-mean warming.

The moist thermal wind contribution from the change in dry entropy gradient and moist adiabatic adjustment (second and third terms on right hand side of (2)) exhibit opposing behavior. The dry entropy gradient response contributes to the fast-get-faster response (green line, Fig. 4a) consistent with mixing across a stronger latitudinal density gradient aloft resulting in larger anomalies and hence, larger longitudinal density gradients and hence, stronger meridional winds. This behavior dominates the density gradient change aloft (Supplementary Fig. 12). However, it is opposed by moist adiabatic adjustment (blue line, Fig. 4a) that leads to fast winds getting slower due to latent heat release aloft weakening the vertical temperature gradient, which dominates the density gradient in the lower atmosphere (Supplementary Fig. 12). This opposing behavior is consistent with what was found for the response of fast upper-level eastward jet stream winds [16, see their Supplementary Fig. 2].

The results show the fast-get-faster mechanism, first revealed for the upper-level eastward jet stream wind, applies to the upper-level meridional wind in the extratropics and implies increased waviness under climate change. The intuition is that all density contrasts steepen under climate change because of the multiplicative CC relation (Fig. 1c). In the case of longitudinal density contrasts driven by dynamics the interpretation is consistent with the analog approach of extreme events. In that approach, a historical extreme event is boosted under global warming[47].

Fast mid-level meridional winds get slower in the Northern Hemisphere

Mid-level (500 hPa) jet stream waviness, where most previous studies have focused, does not exhibit a fast-get-faster response under climate change. It exhibits the opposite: a fast-get-slower response but only in the Northern Hemisphere. The tails of the mid-level meridional wind distribution decrease ~3 times more than the response of the average of the absolute value of upper-level waviness under climate change (Fig. 5a). (Note the average of the absolute value of mid-level meridional wind decreases under climate change). This decrease of fast mid-level meridional jet stream wind implies decreased waviness. The decrease is robust across the Northern Hemisphere (see NH in Fig. 5b) for different seasons (see NH winter from October to March and NH summer from April to September in Fig. 5b) and longitudinal sectors (see North America NAm and Eurasia Eur in Fig. 5b). However, the mid-level waviness response is weak in the Southern Hemisphere (see SH in Fig. 5b), in models without ocean coupling (see AMIP in Fig. 5b) and does not occur in models without land and sea ice (see AQUA in Fig. 5b). The results suggest the mid-level waviness response is sensitive to sea ice loss and polar amplification of surface temperature, which do not occur under climate change in the Southern Hemisphere and in atmosphere-only and aquaplanet models with prescribed uniform sea surface temperature warming and no change in sea ice[48,49] (Supplementary Fig. 9).

Once again MCI cannot capture the response of mid-level waviness extremes because the index is bounded by ±1 (Supplementary Fig. 13a). Mid-level waviness decreases under climate change (Supplementary Fig. 13a). In this case the decrease is mostly dominated by the change in the numerator not the denominator (Supplementary Fig. 13b, c), which explains the good agreement with waviness defined using the mid-level meridional jet stream wind. Mid-level LWA also decreases (black line, Supplementary Fig. 8b) but the response is not robust across the model ensemble (shading, Supplementary Fig. 8b).

The fact that mid-level waviness exhibits the fast-get-slower response only in the Northern Hemisphere suggests a possible role for Arctic sea ice loss and Arctic Amplification. We once again use targeted climate model

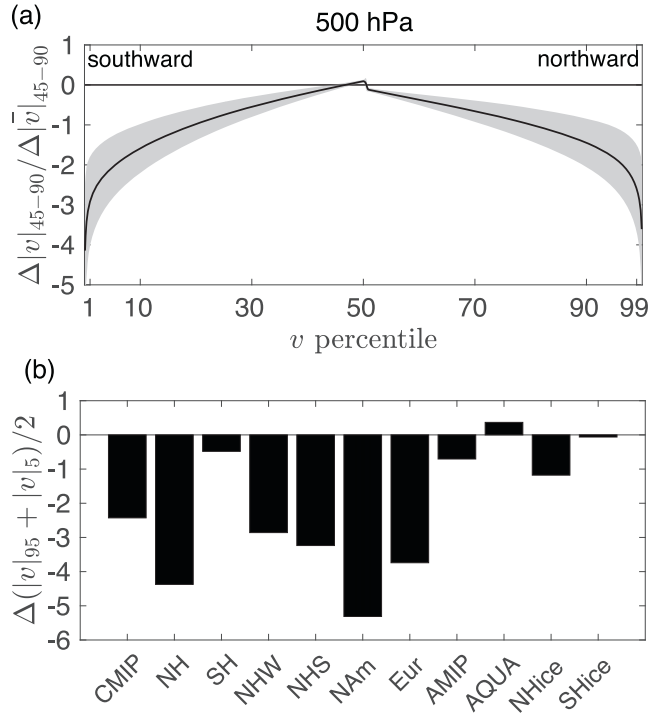

Fig. 5 | Wavy mid-level jet stream winds under climate change. a Response of the extratropical (45–90°) mid-level (500 hPa) jet stream waviness distribution in both hemispheres across percentiles relative to the average of the absolute value of upper-level waviness ($|\overline{v}|$). Data are presented as multi-model-mean (thick line) ± one standard deviation of the response across the model ensemble (shading). **b** Multi-model mean amplification of extreme waviness (average of response for >95th and <5th percentiles) relative to the average of the absolute value of upper-level waviness ($|\overline{v}|$) for coupled models in different seasons in the Northern Hemisphere (winter NHW and summer NHS), across longitudinal sectors (North America NAm 180°W–140°W and Eurasia Eur 40°W–180°E), across different model configurations (coupled CMIP, uncoupled AMIP, aquaplanet AQUA) and in response to Arctic Sea ice loss in the Northern and Southern Hemispheres (NHice and SHice).

simulations that impose end-of-century Arctic sea ice loss without changes in greenhouse gases to quantify the impact of Arctic Sea ice loss[42,43] (see "Methods"). Just as for upper-level waviness, in response to Arctic sea ice loss mid-level waviness exhibits a fast-get slower response (see NHice, SHice in Fig. 5b). Thus, Arctic sea ice loss is important for the decrease of mid-level waviness under climate change. The decrease of mid-level waviness is consistent with a weakening of the midlatitude circulation measured by baroclinic activity, including eddy kinetic energy and transient eddy moist static energy transport, in response to sea ice loss[50].

The fast-get-slower response of mid-level waviness under climate change is captured by moist thermal wind defined at mid-levels (250 hPa replaced by 500 hPa in equation (2)) (black line, Fig. 4b) consistent with the wind distribution being dominated by the geostrophic component (Supplementary Fig. 10b). In this case the fast-get-slower response results from the dry entropy gradient and moist adiabatic adjustment responses (green and blue lines, Fig. 4b) working together to dominate over the moist-get-moister contribution (orange line, Fig. 4b). The dry entropy gradient and moist adiabatic adjustment contributions reflect the impact of diabatic processes, including latent heat release, on climate change in the Arctic (Supplementary Fig. 12)[51,52]. One interpretation is that Arctic sea ice loss induces changes in moisture and diabatic heating over the pole and mixing across a weaker latitudinal density gradient results in weaker anomalies and hence, weaker longitudinal density gradients and hence, weaker meridional winds. This interpretation is consistent with the dry entropy gradient contribution exhibiting a fast-get-slower response (green line, Fig. 4b), and the fast-get-slower response not emerging with only vertically-varying global-mean warming and no change in horizontal temperature gradient.

Emergence of fast-get-faster and fast-get-slower signals

The fast-get-faster response of upper-level waviness at the end of 21st century is robust across hemispheres, seasons, longitudinal sectors and model complexity (Fig. 3b). Over the satellite era (1980 to 2022) the linear trend in the upper-level fast-get-faster index (trend of meridional wind tails average of >95th and <5th percentiles) is positive for the reanalysis mean for both hemispheres (black lines, Fig. 6a, b). According to the Mann-Kendall test the null hypothesis of the absence of a trend can be rejected at 0.05 level for the reanalysis-mean in the Southern ($p = 0.00$) and Northern ($p = 0.03$) hemispheres. The multi-model mean of the climate model ensemble also exhibits a positive trend over the satellite era for both hemispheres across different scenarios (colored lines, Fig. 6a, b). According to the Mann-Kendall test the null hypothesis of the absence of a trend can be rejected at the 0.05 level for the Southern ($p = 0.00$) and Northern ($p = 0.00$) Hemispheres. The models predict a continuation of the linear trend into the middle of the century.

While the climate model ensemble mean trend is statistically significant, the ensemble spread of climate model trends is significant, especially in the Northern Hemisphere. In particular, some models do not exhibit a significant trend (open circles, Fig. 6c, d). However, all of the models suggest a statistically significant linear trend by 2050. A similar result is seen for reanalysis data where JRA55 exhibits a significant trend ($p = 0.01$ closed circles, Fig. 6d) in fast-get-faster index in the Northern Hemisphere but ERA5 does not ($p = 0.09$ open circles, Fig. 6d). This suggests that while there is a statistically significant reanalysis-mean signal in both hemispheres, the signal is less robust in the Northern Hemisphere possibly because there is more noise (internal climate variability). Interestingly recent trends capture the asymmetry between the hemispheres with a larger trend in fast-get-faster index in the Northern Hemisphere similar to the end of the century (Fig. 3b).

Over the satellite era (1980 to 2022) the reanalysis-mean linear trend in the mid-level fast-get-faster index is negative for the Northern Hemisphere and near zero for the Southern Hemisphere (Supplementary Fig. 14). This is consistent with observed polar amplification of surface temperature only occurring in the Arctic[53,54]. According to the Mann-Kendall test the null hypothesis of the absence of a trend can be rejected at 0.05 level for the reanalysis-mean in the Northern Hemisphere ($p = 0.02$) but not the Southern Hemisphere ($p = 0.28$). However, the trends in individual reanalyses are not robust in the Northern Hemisphere ($p = 0.00$ in JRA55 and $p = 0.16$ in ERA5). The lack of robustness is consistent with recent work reaching different conclusions on mid-level waviness trends[21].

Discussion

We have shown the fast-get-faster response, recently uncovered for the upper-level eastward jet stream wind, also occurs for the upper-level meridional jet stream wind in the extratropics (45–90°). The fast-get-faster meridional wind signal is very robust. It emerges under climate change across all models, both hemispheres, all seasons, different regions and across the model hierarchy. Thus, climate models project a wavier upper-level extratropical jet stream under climate change. The increased waviness reflects the response of synoptic features like Rossby wave packets (Fig. 2a–d) under climate change, which occur regionally.

Arctic Sea ice loss does not drive the fast-get-faster upper-level waviness response. Instead it is explained by the same CC mechanism underlying the recently uncovered fast-get-faster response of the upper-level eastward jet stream under climate change. In particular, the results show dynamically-driven longitudinal density contrasts underlying historical waviness in the 20th century are amplified under climate change. The amplification occurs because the longitudinal density contrast associated with fast meridional wind involves air on one side "holding" more moisture (Fig. 1a, b) and the contrast steepens under climate change (blue to orange in Fig. 1c). The response involves a multiplicative increase (~2% per degree of global mean

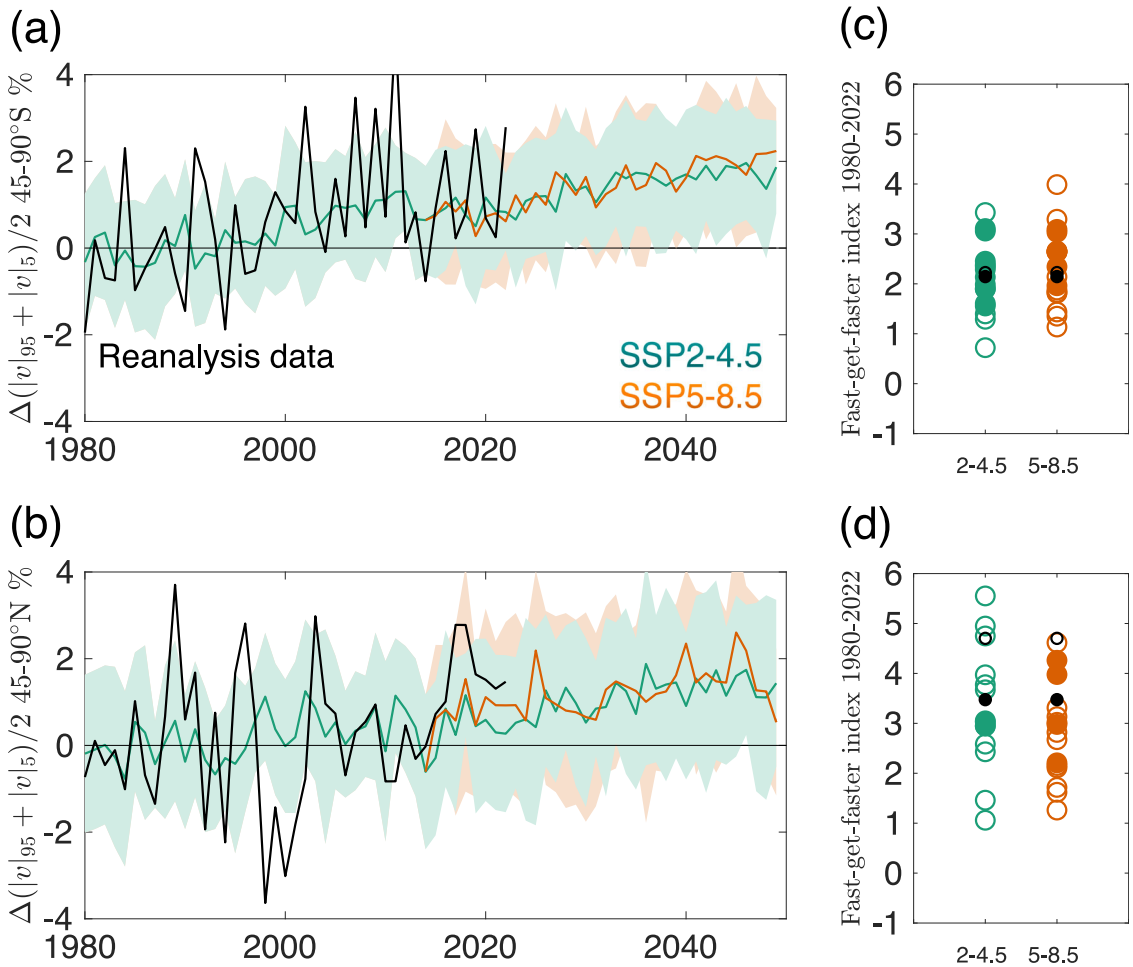

Fig. 6 | Emergence of wavy-get-wavier signal. Time series of fractional changes (relative to the 1980–2000 period) in extreme northward and southward (average of >95th and <5th percentile) upper-level waviness in reanalysis-mean (black line) and climate models for different emission scenarios (colored lines) for the (**a**) Southern and (**b**) Northern Hemisphere extratropics in the satellite era (1980–2022). Shading indicates one standard deviation across the model ensemble. Linear trends of fractional changes in the fast-get-faster index (trend in the extreme northward and southward waviness relative to trends in average waviness) in different reanalysis products (black circles) and climate models for different scenarios (green, orange circles) for the (**c**) Southern and (**d**) Northern Hemisphere extratropics. Statistically significant trends are indicated by closed circles.

surface air temperature) of waviness following the CC relation. The multiplicative increase is key: if the historical end of 20th century distribution is multiplied by 2%/K the fast-get-faster upper-level waviness response emerges. We note that while the fast-get-faster responses of the eastward and meridional jet stream winds are connected to the same underlying mechanism their responses are not significantly correlated on the daily time scale at individual spatial locations ($R = 0.01$, Supplementary Fig. 3) consistent with them being connected to distinct spatial gradients.

Our results show that while the fast-get-faster response is robust at upper levels, mid-level waviness exhibits a fast-get-slower response under climate change but only in the Northern Hemisphere. Thus, mid-level waviness in the Northern Hemisphere decreases under climate change and the decrease is robust across four different waviness metrics (meridional wind, MCI, LWA, sinuosity)[6,22,23]. The fast-get-slower response, reflecting the waviness decrease, emerged only in the presence of Arctic Sea ice loss and Arctic Amplification. It does not emerge under global warming in the Southern Hemisphere, in atmosphere-only and aquaplanet configurations with prescribed sea surface temperature, which exhibit very weak polar amplification of surface temperature. Thus, the upper-level fast-get-faster response emerges under global warming but the fast-get-slower response only emerges under Arctic Sea ice loss and Arctic Amplification.

The fast-get-slower response of mid-level waviness under climate change is related to reduced density contrasts associated with a reduced longitudinal dry entropy gradient, which is affected by latent heat release along with other forms of diabatic heating, and moist adiabatic adjustment, which weakens the vertical temperature gradient. The mid-level response seems to be consistent with Arctic sea ice loss inducing changes in moisture and diabatic heating over the pole[51,52] and mixing across a weaker latitudinal density gradient resulting in weaker anomalies and hence, weaker longitudinal density gradients and hence, weaker meridional winds. Thus, while previous work examining changes in daily jet stream waviness averaged over monthly timescales argued that Arctic Sea ice loss and Arctic amplification increase waviness[5,21,30], our results do not support the hypothesis that Arctic sea ice loss and Arctic Amplification lead to increased waviness.

Overall the results show moist processes can be used to understand changes in waviness throughout the atmosphere. The importance of moisture means that the results of dry atmosphere model simulations [e.g.[55]], while still useful, should be interpreted with caution. Furthermore, the results suggest that separating the climate change response into "thermodynamic" (depends on global-mean temperature and leads to a moisture increase) and "dynamic" (independent of global-mean temperature)[56,57] may be misleading. The fast-get-faster response shows changes in thermodynamics via moisture lead to balanced dynamical responses. More appropriate terminology would be "moisture", including balanced geostrophic dynamics, and "convergence", including ageostrophic dynamics[58].

Our results also show that jet stream waviness measured using upper-level meridional wind exhibits a more robust response under climate change than other local waviness metrics such as MCI[5] and LWA[38]. The diverging consensus on waviness changes[21] may be in part a result of using different indices to measure waviness as highlighted by[24,55]. In particular, MCI is bounded by ±1 and thus cannot exhibit changes in extreme values. In addition, MCI is nonlinear and the numerator and denominator exhibit competing responses under climate change. The LWA metric of waviness exhibits similar behavior to waviness defined using meridional wind but its response is not robust across the model ensemble.

Finally, previous work has argued that waviness impacts surface extremes through advection[9–15]. The significant decrease in wintertime temperature variability in the Northern Hemisphere in recent decades[13] is consistent with the recent decrease in mid-level waviness. However, many factors affect extreme weather at the surface, including local (land surface, boundary layer wind, surface radiation, etc.) and non local (wind above boundary layer, radiation in the free atmosphere, clouds, etc.) factors. Waviness aloft is a non-local factor and can impact surface extremes through vertically-integrated meridional advection. When waviness exhibits opposing behavior in the vertical (baroclinic vertical structure) the vertically-integrated meridional advection would potentially be small compared to when there is no tug of war (close to barotropic vertical structure) above the boundary layer. The opposing responses of upper- and mid-level waviness under climate change in the Northern Hemisphere suggest the impact of waviness changes at the surface may be small there whereas the impacts may be stronger in the Southern Hemisphere. Further work is needed to understand the impact of waviness changes on surface extremes across different regions and seasons.

Methods

Reanalysis and climate model data

We use daily meridional wind (va) and temperature (ta) data from 18 CMIP6 (Supplementary Table 1) models. We use coupled model simulations under historical, ssp5-8.5 and ssp2-4.5 forcing, prescribed sea surface temperature atmosphere-only model simulations for the climatology and with +4 K sea surface temperature warming, and finally prescribed sea surface temperature aquaplanet model simulations for an idealized climatology and with +4 K sea surface temperature warming. We also make use of simulations with Arctic Sea ice loss (Supplementary Table 2)[42,43].

We also use daily zonal wind data from the ERA5[41] and JRA55[59] reanalysis from 1980 to 2022. For ERA5 and JRA55 the daily zonal wind data was constructed from hourly data.

The magnitude of extremes at a given percentile are known to depend on spatial resolution[60]. In order to ensure a like-for-like comparison we examine the reanalysis and climate model extremes on the same spatial grid. The 37 pressure-level reanalysis data is sub-sampled onto the same 8 pressure level climate model vertical grid (1000, 925, 850, 700, 500, 300, 250, 200, 150, 100, 50, 10 hPa). For the horizontal grid, we interpolate all data onto a 1.5 by 1.5 degree grid using cubic spline interpolation.

We divide all days in to winter (from October to March in the Northern Hemisphere and October to March in the Southern Hemisphere) and summer (from April to September in the Northern Hemisphere and October to March in the Southern Hemisphere) seasons.

Statistical tests

The satellite-era linear trends (Fig. 5) were quantified by a least-squares linear regression model. The statistical significance of the linear trend was quantified using a Mann-Kendall test which tests the null hypothesis of the absence of a trend.

Moist thermal wind

Moist thermal wind can be derived for a saturated atmosphere by writing the specific volume $\alpha = \alpha(s^*, p)$ where s^* is the saturated moist entropy, which is conserved under moist reversible processes, and p is pressure[45,46]. The longitudinal gradient of specific volume, which appears in the equation for thermal wind [equation (2)] can be written as

$$\left(\frac{\partial \alpha}{\partial \lambda}\right)_p = \left(\frac{\partial \alpha}{\partial s^*}\right)_p \frac{\partial s^*}{\partial \lambda}. \tag{4}$$

Saturated moist entropy satisfies the first law of thermodynamics

$$Tds^* = du + pd\alpha + Ldq^* \tag{5}$$

which can be written as a function of saturated moist enthalpy $h^* \equiv u + p\alpha + Lq^*$ such that

$$dh^* = Tds^* + \alpha dp. \tag{6}$$

These relationships imply

$$\left(\frac{\partial h^*}{\partial p}\right)_{s^*} = \alpha \tag{7}$$

$$\left(\frac{\partial h^*}{\partial s^*}\right)_p = T \tag{8}$$

Since $q^*(T, p)$ and $h^*(s^*, p)$ we have equality of mixed partial derivatives

$$\left(\frac{\partial}{\partial s^*}\right)_p \left(\frac{\partial h^*}{\partial p}\right)_{s^*} = \left(\frac{\partial}{\partial p}\right)_{s^*} \left(\frac{\partial h^*}{\partial s^*}\right)_p \tag{9}$$

and upon substitution into equations (7)–(8) we obtain the Maxwell relation

$$\left(\frac{\partial \alpha}{\partial s^*}\right)_p = \left(\frac{\partial T}{\partial p}\right)_{s^*} \tag{10}$$

where the right hand side is the moist adiabatic lapse rate. The meridional gradient of specific volume is

$$\left(\frac{\partial \alpha}{\partial \lambda}\right)_p = \left(\frac{\partial T}{\partial p}\right)_{s^*} \frac{\partial s^*}{\partial \lambda}. \tag{11}$$

which becomes moist thermal wind upon substitution of $\left(\partial\alpha/\partial\lambda\right)_p$ into the thermal wind equation:

$$v_{Tm} \equiv -\int_{p_s}^{250\,\mathrm{hPa}} \frac{1}{fa\cos\phi}\frac{\partial \alpha}{\partial \lambda} dp = \int_{p_s}^{250\,\mathrm{hPa}} \frac{1}{fa\cos\phi}\left(\frac{\partial T}{\partial p}\right)_{s^*} \frac{\partial s^*}{\partial \lambda} dp. \tag{12}$$

The physical interpretation of moist thermal wind is that changes in the longitudinal density gradient in a moist atmosphere can be influenced by changes the meridional gradient of saturation entropy and the impact of latent heat release aloft via the moist adiabatic lapse rate.

Reporting summary

Further information on research design is available in the Nature Portfolio Reporting Summary linked to this article.

Data availability

The data used in the manuscript are publicly available: CMIP6, CMIP5, and ERA5.

Code availability

The codes used in the manuscript are available at https://doi.org/10.5281/zenodo.8428075 [ref. 5].

Received: 20 May 2024; Accepted: 21 October 2024;
Published online: 03 November 2024

References

1. Wallace, J. M. & Hobbs, P. V. Atmospheric science: an introductory survey. *Academic Press*, 504 (2006).
2. Holton, J. M. & Hakim, G. An introduction to dynamic meteorology. *Academic Press*, 552 (2012).
3. Vallis, G. K. Atmospheric and oceanic fluid dynamics fundamentals and large-scale circulation. *Cambridge University Press*, https://doi.org/10.1017/CBO9780511790447 (2006).
4. Held, I. M. & Hou, A. Nonlinear axially symmetric circulations in a nearly inviscid atmosphere. *J. Atmos. Sci.* **37**, 515–533 (1980).
5. Francis, J. A. & Vavrus, S. J. Evidence for a wavier jet stream in response to rapid Arctic warming. *Environ. Res. Lett.* **10**, 014005 (2015).
6. Cattiaux, J., Peings, Y., Saint-Martin, D. Trou-Kechout, N., & Vavrus, S. J., Sinuosity of midlatitude atmospheric flow in a warming world. *Geophys. Res. Lett*. https://doi.org/10.1002/2016GL070309 (2016).
7. Röthlisberger, M., Pfahl, S., & Martius, O., Regional-scale jet waviness modulates the occurrence of midlatitude weather extremes. *Geophys. Res. Lett*. https://doi.org/10.1002/2016GL070944 (2016).
8. Martin, J. Recent trends in the waviness of the Northern Hemisphere wintertime polar and subtropical jets. *J. Geophys. Res*. https://doi.org/10.1029/2020JD033668 (2021).
9. Buehler, T., Raible, C. C. & Stocker, T. F. The relationship of winter season North Atlantic blocking frequencies to extreme cold or dry spells in the ERA-40. *Tellus* **63**, 212–222 (2011).
10. Pfahl, S. & Wernli, H., Quantifying the relevance of atmospheric blocking for co-located temperature extremes in the Northern Hemisphere on (sub-)daily time scales. *Geophys. Res. Lett*. 39, https://doi.org/10.1029/2012GL052261 (2012)
11. Wang, S.-Y., Davie, R. E.s & Gillies, R. R., Identification of extreme precipitation threat across midlatitude regions based on short-wave circulations. *J. Geophys. Res*. https://doi.org/10.1002/jgrd.50841 (2013).
12. Coumou, D., Petoukhov, V., Rahmstorf, S., Petri, S. & Schellnhuber, H. J. Quasi-resonant circulation regimes and hemispheric synchronization of extreme weather in boreal summer. *Proc. Natl Acad. Sci. USA* **111**, 12331–12336 (2014).
13. Screen, J. A. Arctic amplification decreases temperature variance in northern mid- to high-latitudes. *Nat. Clim. Change* **4**, 577–582 (2014).
14. Martineau, P., Chen, G. & Burrows, D. A. Wave events: climatology, trends, and relationship to Northern Hemisphere winter blocking and weather extremes. *J. Clim.* **30**, 5675–5697 (2017).
15. Sun, W., Hess, P., Chen, G. & Tilmes, S. How waviness in the circulation changes surface ozone: a viewpoint using local finite-amplitude wave activity. *Atmos. Chem. Phys.* **19**, 12917–12933 (2019).
16. Shaw, T. A. & Miyawaki, O. Fast upper-level jet stream winds get faster under climate change. *Nat. Clim. Change*, https://doi.org/10.1038/s41558-023-01884-1 (2023).
17. Shaw, T. A. & Voigt, A. What can moist thermodynamics tell us about circulation shifts in response to uniform warming? *Geophys. Res. Lett*., https://doi.org/10.1002/2016GL068712 (2016).
18. Barnes, E. A. & Screen, J. The impact of Arctic warming on the midlatitude jet-stream: Can it? Has it? Will it? *WIREs Clim. Change* **6**, 277–286 (2015).
19. Hoskins, B. J. & Woollings, T. Persistent extratropical regimes and climate extremes. *Curr. Clim. Change Rep.* **1**, 115–124 (2015).
20. Francis, J. A. Why are Arctic linkages to extreme weather still up in the air? *Bull. Amer. Met. Soc*. https://doi.org/10.1175/BAMS-D-17-0006.1 (2017).
21. Cohen, J. et al. Divergent consensuses on Arctic amplification influence on midlatitude severe winter weather. *Nat. Clim. Change*, https://doi.org/10.1175/BAMS-D-17-0006.1 (2020).
22. Nie, Y., Chen, G., Lu, J., Zhou, W., & Zhang, Y. Constraining the varied response of Northern Hemisphere winter circulation waviness to climate change. *Geophys. Res. Lett.* https://doi.org/10.1029/2022GL102150 (2023).
23. Yamamoto, A. & Martineau, P. On the driving factors of the future changes in the wintertime Northern-Hemisphere atmospheric waviness. *Geophys. Res. Lett*. https://doi.org/10.1029/2024GL108793 (2024).
24. Barnes, E. A. Revisiting the evidence linking Arctic amplification to extreme weather in midlatitudes. *Geophys. Res. Lett.* **40**, 4734–4739 (2013).
25. Blackport, R. & Screen, J. A. Insignificant effect of Arctic amplification on the amplitude of midlatitude atmospheric waves. *Sci. Adv.* **6**, eaay2880 (2020).
26. Blackport, R., Fyfe, J. & Screen, J. A. Decreasing subseasonal temperature variability in the northern extratropics attributed to human influence. *Nat. Geosci.* **14**, 719–723 (2021).
27. Manabe, S. & Weatherald, R. T. The effects of doubling the CO_2 concentration on the climate of a general circulation model. *J. Atmos. Sci.* **32**, 3–15 (1975).
28. Held, I. M. Large-scale dynamics and climate change. *Bull. Amer. Met. Soc*. **74**, https://doi.org/10.1175/1520-0477 (1993).
29. Pithan, F. & Mauritsen, T. Arctic amplification dominated by temperature feedbacks in contemporary climate models. *Nat. Geosc.* https://doi.org/10.1038/NGEO2071 (2014).
30. Francis, J. A. & Vavrus, S. J. Evidence linking Arctic amplification to extreme weather in mid-latitudes. *Geophys. Res. Lett*. **39**, https://doi.org/10.1029/2012GL051000 (2012).
31. Moon, W., B.-M., Kim, G.-H., Yang, & Wettlaufer, J. S. Wavier jet streams driven by zonally asymmetric surface thermal forcing. *Proc. Nat. Acad. Sci*. https://doi.org/10.1073/pnas.2200890119 (2022).
32. Schneider, T., Bischoff, T. & Plotka, H. Physics of changes in synoptic midlatitude temperature variability. *J. Clim.* **28**, 2312–2331 (2015).
33. Held, I. M. The gap between simulation and understanding in climate modeling. *Bull. Amer. Met. Soc*. https://doi.org/10.1175/BAMS-86-11-1609 (2005).
34. Vallis, G. K. Response of the large-scale structure of the atmosphere to global warming. *Q. J. Roy. Met. Soc.* **141**, 1479–1501 (2015).
35. Shaw, T. A. Mechanisms of future predicted changes in the zonal mean mid-latitude circulation. *Curr. Clim. Change Rep.* **5**, 345–357 (2019).
36. Wills, R. C. J., White, R. H. & Levine, X. J. Northern Hemisphere stationary waves in a changing climate. *Curr. Clim. Change Rep.* **5**, 372–389 (2019).
37. Eyring, V. et al. Overview of the coupled model intercomparison project phase 6 (CMIP6) experimental design and organization. *Geosci. Model Dev.* **9**, 1937–1958 (2016).
38. Chen, G., Lu, J., Burrows, D. A. & Leung, L. R. Local finite-amplitude wave activity as an objective diagnostic of midlatitude extreme weather. *Geophys. Res. Lett.* **42**, 10952–10960 (2019).
39. Virth, V., Reimer, M., Chang, E. K. M., & Martius, O. Rossby wave packets on the midlatitude waveguide—a review. *Mon. Wea. Rev*. https://doi.org/10.1175/MWR-D-16-0483.1 (2018).
40. Woollings, T. et al. Blocking and its response to climate change. *Curr. Clim. Change Rep.* **4**, 287–300 (2018).
41. Hershbach, H. et al. The ERA5 global reanalysis. *Quart. J. Roy. Met. Soc*. **146**, https://doi.org/10.1002/qj.3803 (2020).
42. Smith, D. M. et al. The polar amplification model Intercomparison project (PAMIP) contribution to CMIP6: Investigating the causes and consequences of polar amplification. *Geosci. Model Develop.* https://doi.org/10.5194/gmd-12-1139-2019 (2019).
43. Kang, J., Shaw, T. A., & Sun, L. Arctic sea ice loss weakens Northern Hemisphere summertime storminess but not until the late 21st century. *Geophys. Res. Lett*. https://doi.org/10.1029/2022GL102301 (2023).
44. Lee, S., Williams, P. D. & Frame, T. Increased shear in the North Atlantic upper-level jet stream over the past four decades. *Nature* **572**, 639–642 (2019).

45. Emanuel, K. A. An air-sea interaction theory for tropical cyclones. Part I. *J. Atmos. Sci.* **43**, 585–604 (1986).
46. Emanuel, K. A. On thermally direct circulation in moist atmospheres. *J. Atmos. Sci.* **52**, 1529–1534 (1995).
47. Faranda, D., Vrac, M., Yiou, P., Jezequel, A., & Thao, S. Changes in future synoptic circulation patterns: consequences for extreme event attribution. *Geophys. Res. Lett*. https://doi.org/10.1029/2020GL088002 (2020).
48. Voigt, A. & Shaw, T. A. Circulation response to warming shaped by radiative changes of clouds and water vapour. *Nat. Geosc*. https://doi.org/10.1038/NGEO2345 (2015).
49. Karpechko, A. & Manzini, E. Arctic stratosphere dynamical response to global warming. *J. Clim.* **30**, 7071–7086 (2017).
50. Shaw, T. A. & Smith, Z. The midlatitude response to polar sea ice loss: idealized slab-ocean aquaplanet experiments with thermodynamic sea ice. *J. Clim.* **35**, 2633–2649 (2022).
51. Pithan, F. & Jung, T. Arctic amplification of precipitation changes—the energy hypothesis. *Geophys. Res. Lett*. https://doi.org/10.1029/2021GL094977 (2021).
52. Miyawaki, O., Shaw, T. A. & Jansen, M. F. The emergence of a new wintertime Arctic energy balance regime. *Environ. Res. Clim.* https://doi.org/10.1088/2752-5295/aced63 (2023).
53. Hahn, L. C., Armour, K. C., Zelinka, M. D., Bitz, C. M. & Donohoe, A. Contributions to polar amplification in CMIP5 and CMIP6 models. *Front. Earth Sci*. https://doi.org/10.3389/feart.2021.710036 (2020).
54. Rantanen, M. et al. The Arctic has warmed nearly four times faster than the globe since 1979. *Comm. Earth Environ*. https://doi.org/10.1038/s43247-022-00498-3 (2022).
55. Geen, R. et al. An Explanation for the metric dependence of the midlatitude jet-waviness change in response to polar warming. *Geophys. Res. Lett*. https://doi.org/10.1029/2023GL105132 (2023).
56. Seager, R., Naik, N. & Vecchi, G. A. Thermodynamic and dynamic mechanisms for large-scale changes in the hydrological cycle in response to global warming. *J. Clim.* **23**, 4651–4668 (2010).
57. Shepherd, T. G. Atmospheric circulation as a source of uncertainty in climate change projections. *Nat. Geosci.* https://doi.org/10.1038/NGEO2253 (2014).
58. Neelin, J. D. et al. Precipitation extremes and water vapor relationships in current climate and implications for climate change. *Curr. Clim. Change Rep.* **8**, 17–33 (2022).
59. Kobayashi, S. et al. The JRA-55 reanalysis: general specifications and basic characteristics. *J Meteorol. Soc. Japan* **93**, 5–48 (2015).
60. Chen, C. T. & Knutson, T. On the verification and comparison of extreme rainfall indices from climate models. *J. Clim.* **21**, 1605–1621 (2008).

Acknowledgements

This work was completed in part with resources provided by the University of Chicago's Research Computing Center. We acknowledge the World Climate Research Programme's Working Group on Coupled Modelling, which is responsible for CMIP, and we thank the climate modeling groups listed in Supplementary Table 1 for producing and making available their model output. For CMIP the US Department of Energy's Program for Climate Model Diagnosis and Intercomparison provides coordinating support and led development of software infrastructure in partnership with the Global Organization for Earth System Science Portals. The authors thank J. Kang for providing access to the Arctic Sea ice loss simulation data and three anonymous reviewers whose comments significantly improved the manuscript.

Author contributions

T.A.S. conceived of the study and analyzed the data. O.M. acquired the data. T.A.S., O.M., H.-H.C., and R.B. discussed the results and wrote the manuscript.

Competing interests

The authors declare no competing interests.

Additional information

Supplementary information The online version contains supplementary material available at https://doi.org/10.1038/s43247-024-01819-4.

Correspondence and requests for materials should be addressed to Tiffany A. Shaw.

Peer review information *Communications Earth & Environment* thanks Woosok Moon and the other, anonymous, reviewer(s) for their contribution to the peer review of this work. Primary Handling Editors: Kyung-Sook Yun and Alireza Bahadori. A peer review file is available.